J. Math. Biol.
DOI 10.1007/s00285-014-0792-9

Mathematical Biology

Spatial pattern formation in the lung

Graham M. Donovan · Thibaut Kritter

Received: 18 August 2013 / Revised: 3 March 2014

Abstract Clustered ventilation defects are a hallmark of asthma, typically seen via imaging studies during asthma attacks. The mechanisms underlying the formation of these clusters is of great interest in understanding asthma. Because the clusters vary from event to event, many researchers believe they occur due to dynamic, rather than structural, causes. To study the formation of these clusters, we formulate and analyze a lattice-based model of the lung, considering both the role of airway bistability and a mechanism for organizing the spatial structure. Within this model we show how and why the homogeneous ventilation solution becomes unstable, and under what circumstances the resulting heterogeneous solution is a clustered solution. The size of the resulting clusters is shown to arise from structure of the eigenvalues and eigenvectors of the system, admitting not only clustered solutions but also (aphysical) checkerboard solutions. We also consider the breathing efficiency of clustered solutions in severely constricted lungs, showing that stabilizing the homogeneous solution may be advantageous in some circumstances. Extensions to hexagonal and cubic lattices are also studied.

Keywords Asthma · Heterogeneity · Bistability · Airway hyper-responsiveness · Lattice dynamical system

Mathematics Subject Classification 92B05 · 34D20

GMD acknowledges the support of the National Institutes of Health via NHLBI HL103405.

G. M. Donovan (✉)
Department of Mathematics, University of Auckland, Auckland, New Zealand
e-mail: g.donovan@auckland.ac.nz

T. Kritter
École Normale Supérieure de Cachan, Cachan, France

Published online: 09 May 2014

1 Introduction

Asthma is a widespread disease, with mortality and morbidity which may startle those unfamiliar with its scope—for example, there are 300 million sufferers worldwide, and 250,000 deaths annually (World Health Organization 2007). Asthma is fundamentally a disease of reversible airway constriction, and one of its hallmarks is ventilation heterogeneity, or more specifically, clustered ventilation defects (VDs). That is, imaging studies of asthmatic lungs during asthma attacks typically show clustered regions of very low ventilation, as might be expected in a subject struggling to breathe, but interestingly also exhibit hyper-ventilated regions (see Fig. 1). Because these clusters vary from event to event, even for the same patient, many researchers believe that the causes are dynamic rather than structural (e.g. Venegas et al. 2005).

This dynamic clustering has motived interest in models of individual airways which exhibit bistability between open and closed airway states (Anafi and Wilson 2001; Venegas et al. 2005; Lambert et al. 1982; Donovan et al. 2012). In general this is the result of interaction between (passive) airway wall mechanics and the dynamics of airway smooth muscle (ASM), which surrounds each airway and serves to constrict the airway when the muscle is activated. However, this bistability is only a partial answer to the question of how clustered VDs form, although it is highly suggestive. That is, if individual airways may be open or closed, dependent upon history but under equivalent conditions, then this can explain heterogeneity but not the spatial clustering. What principle organises the spatial structure? This question has been partially answered by Anafi and Wilson (2001), and Venegas et al. (2005), who suggest that pressures felt by any individual airway in the lung are related to the inflation of nearby lung tissue. The latter group has demonstrated via direct numerical simulations that this

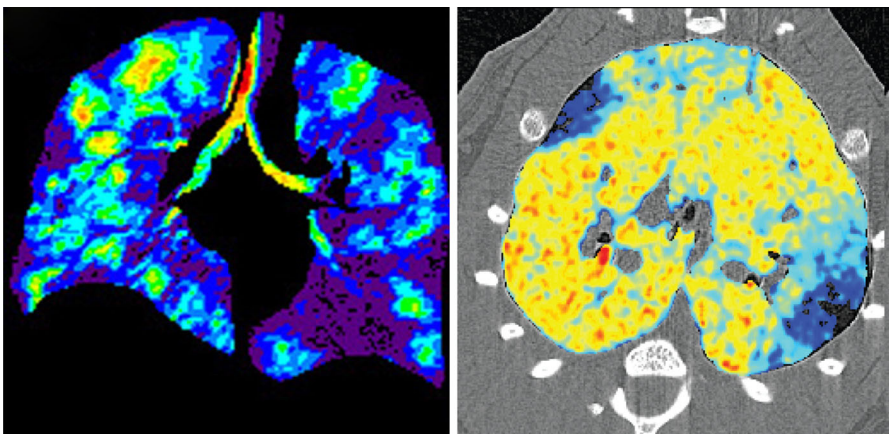

Fig. 1 Typical asthmatic clustered ventilation defects from imaging studies. *Left panel* voxel fractional ventilation map from hyperpolarized 3he MRI, colored from *red* (high) to *black* (low) reproduced with permission from Tzeng et al. (2009); *right panel* xenon density from K-edge subtraction synchrotron imaging, colored from red (high, 4.0 mg/ml) to black (low, 0.0 mg/ml) reproduced with permission from Layachi et al. (2013) (color figure online)

mechanism may be responsible for clustered VDs, at least in an idealised geometry and under certain conditions.

Here we formulate a model of the lung, consisting of a coupled lattice of terminal airway units, (a terminal unit consisting of the terminal conducting bronchiole, with pulmonary acinus) for the purpose of studying the conditions under which clustered ventilation defects arise. The airway units employ the previously known bistability in isolation; furthermore, we consider one possible mechanism of spatial organization wherein neighbouring units are coupled depending on the flow to their neighbours. Analysis of this model allows us to consider the implications of clustered ventilation defects caused via this organising mechanism.

This structure also allows us to consider the role of the mechanism controlling breathing pressures. Consider: when airways constrict, does airflow decrease, or does the driving pressure increase to compensate? We will show that assumptions about the nature of this control have important implications for the formation of clustered ventilation defects. This approach allows a great deal of analysis which lends understanding as to why and how clustered ventilation defects occur in the model.

2 Model

Here we formulate the lattice dynamical system which is the basis of this work. We assume a 2D lattice of terminal airway units, neglecting the airway branching structure (Horsfield et al. 1971) and assuming that each element in the lattice experiences equivalent input conditions.

The internal dynamics of a single terminal unit are described in terms of airway luminal radius r; for the ith lattice element then

$$\dot{r_i} = \rho \left[\Phi(r_i; r_{j_1}, r_{j_2}, r_{j_3}, r_{j_4}) - r_i \right] \tag{1}$$

where $j_{1\ldots4} \in \mathcal{N}_i$ are the coupled (nearest) neighbors. Here we have employed simple first-order relaxation kinetics with a time constant ρ, and the function Φ is based on (static) experimental data for the behaviour of conducting airways. Following Donovan et al. (2012) (who considered a similar construction as an iterated map) we assemble Φ from composition of several existing models in the physiology literature, so that

$$\Phi(r_i; r_{j_1}, r_{j_2}, r_{j_3}, r_{j_4}) = R(P(r_i; r_{j_1}, r_{j_2}, r_{j_3}, r_{j_4}))$$

where $R(P)$ describes airway radius as a function of transmural pressure according to

$$R(P) = \begin{cases} \sqrt{R_i^2(1 - P/P_1)^{-n_1}}, & P \leq 0 \\ \sqrt{r_{imax}^2 - (r_{imax}^2 - R_i^2)(1 - P/P_2)^{-n_2}}, & P > 0 \end{cases} \tag{2}$$

from Lambert et al. (1982) where $R_i, r_{imax}, P_1, P_2, n_1$ and n_2 are parameters from Lambert et al. (1982) with notation adapted from Politi et al. (2010), see Sect. 5. Note that other choices for this radius-pressure relationship are possible, see Sect. 3.8. Here $P(r)$ gives transmural pressure as a function of the radius as

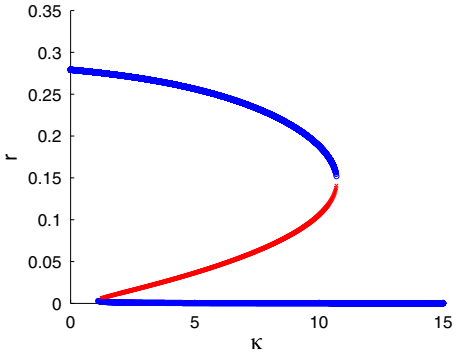

Fig. 2 Typical individual small airway bistability, with "open" and "closed" states (e.g. Affonce and Lutchen 2006; Donovan et al. 2012). *Blue* indicates stable fixed points, red unstable. Note these are the fixed points of Eq. 1 if μ is constant and so the dependence of one airway on its neighbors vanishes (color figure online)

$$P(r_i; r_{j_1}, r_{j_2}, r_{j_3}, r_{j_4}) = P_b - \frac{\kappa R_{ref}}{r_i} + \tau(r_i; r_{j_1}, r_{j_2}, r_{j_3}, r_{j_4}). \tag{3}$$

Here the terms on the right-hand side correspond to a base pressure, the constricting pressure of airway smooth muscle (represented by the smooth muscle pressure κ, with $1/r_i$ from the Laplace law for thin-walled cylinders and R_{ref} as a normalizing reference radius), and the so-called parenchymal *tethering pressure*. This arises from the restoring forces generated by the parenchymal tissue surrounding the airway, and is described by

$$\tau(r_i; r_{j_1}, r_{j_2}, r_{j_3}, r_{j_4}) = 2\mu(r_i; r_{j_1}, r_{j_2}, r_{j_3}, r_{j_4}) \left(\left(\frac{R_{ref} - r_i}{R_{ref}} \right) + 1.5 \left(\frac{R_{ref} - r_i}{R_{ref}} \right)^2 \right) \tag{4}$$

according to Lai-Fook (1979), where μ is the parenchymal shear modulus, which is dependent on lung inflation. With constant μ, this model exhibits a previously-demonstrated bistability (Donovan et al. 2012; Affonce and Lutchen 2006; Lambert et al. 1982), shown as the ASM pressure varies in Fig. 2. Here we introduce the local effect that the shear modulus is a function of the local inflation via mean local flow, so that

$$2\mu(r_i; r_{j_1}, r_{j_2}, r_{j_3}, r_{j_4}) = P_b \frac{A}{5} \left(r_i^4 + \sum_{j \in \mathcal{N}_i} r_j^4 \right) \tag{5}$$

where the 4th power dependence arises from the assumption of quasi-steady Poiseuille flow and the parameter A represents the coupling strength. (Recall that $\mathcal{N}_i$ are the nearest neighbors to element i.) This choice of dependence on local flow, rather than local volume, is a key assumption which enables much of the analysis presented—please see Sect. 6. Note that total closure of airways does not occur (rather, very near closure) and so changes in driving pressure are always transmitted throughout the lattice. (It is worth noting here that we consider only one possible mechanism of spatial organisation, and that others have been proposed; see Sect. 6 for more details.)

Identical units with these dynamics are configured in a square lattice denoted $\mathcal{L}$ of dimensions $N \times N$ with periodic-type boundary conditions. If we assume that P_b is constant, then this is a lattice dynamical system with nearest-neighbour coupling; hence we refer to this as local-only coupling. This corresponds physiologically to the assumption that the pressures driving breathing do not increase to compensate for airway constriction.

If we consider instead that total flow must be maintained despite constriction (e.g. Venegas et al. 2005), and that P_b takes this control role, then by Poisseuille flow we have

$$(P_b(t) - P_0) \sum_{k \in \mathcal{L}} r_k^4(t) = \sigma \hat{Q} \tag{6}$$

with the Poisseuille flow coefficient $\sigma = 8\mu_{dv} L/\pi$ where μ_{dv} is the dynamic viscosity of air and L is the length of a terminal airway. Because we are interested in relative flow, we scale σ to unity and take $P_0 = 0$ so that

$$P_b(t) \sum_{k \in \mathcal{L}} r_k^4(t) = \hat{Q} \tag{7}$$

where $\hat{Q}$ is the target flow taken at reference: $\hat{Q} = P_b(0) N^2 R_{ref}^4$. That is, pressure increases to maintain flow despite constriction. Thus P_b is a function of all elements in the lattice and we have a global coupling term. We will refer to these two distinct cases as *local-only coupling* and *global and local coupling*; this is an important distinction both for the analysis and the qualitative results. Note that other units and parameter values are given in Sect. 5.

To a certain extent, much of the analysis presented is agnostic to many of the model specifics, but instead is based only on

- the intrinsic airway bistability;
- the nearest-neighbour (local) coupling;
- global coupling via breathing control, and
- the relevant partial derivatives, evaluated at the homogeneous fixed points.

As discussed in Sects. 3.8 and 6, at least some modelling assumptions can be relaxed while retaining these features, and the qualitative results.

3 Results and analysis

3.1 Homogeneous vs. clustered solutions

We first consider some numerical results to illustrate the types of solution that one might expect from this system. The most obvious is the homogeneous ventilation solution; that is, all lattice elements equilibrate to the same value. Somewhat less

obviously, clustered ventilation solutions also occur: see Fig. 3 for an example with global and local coupling.

Of course, this is only illustrative and naturally raises the questions: under what conditions does the homogeneous solution lose stability? What sorts of heterogeneous distributions arise?

3.2 Jacobian structure and eigenvalues

To answer the first of these questions we first look to the eigenvalues of the system, which can be obtained because of the structure of the Jacobian arising from the lattice and coupling structure.

3.2.1 Local-only coupling: eigenvalues

Recall that the local-only coupling case takes $P_b =$ constant and represents the state where airway constriction results in reduced flow rather than increased driving pressures.

Here we form the Jacobian using the definitions

$$\alpha = \rho\left(\frac{\partial \Phi}{\partial r_i} - 1\right)$$
$$\beta = \rho\frac{\partial \Phi}{\partial r_j}$$

for compactness of notation, then $\mathcal{J}$ has block structure

$$\mathcal{J} = \begin{bmatrix} A & B & 0 & \dots & 0 & B \\ B & A & B & 0 & \dots & 0 \\ 0 & B & A & B & 0 & \dots \\ \vdots & & \ddots & \ddots & \ddots & \vdots \\ 0 & \dots & 0 & B & A & B \\ B & 0 & \dots & 0 & B & A \end{bmatrix}$$

where the blocks are $N \times N$ (and so $\mathcal{J}$ is $N^2 \times N^2$). The main diagonal blocks are self-similar with

$$A = \begin{bmatrix} \alpha & \beta & 0 & \dots & 0 & \beta \\ \beta & \alpha & \beta & 0 & \dots & 0 \\ 0 & \beta & \alpha & \beta & 0 & \dots \\ \vdots & & \ddots & \ddots & \ddots & \vdots \\ 0 & \dots & 0 & \beta & \alpha & \beta \\ \beta & 0 & \dots & 0 & \beta & \alpha \end{bmatrix}$$

and the off-diagonal blocks B are diagonal matrices with β on the diagonal.

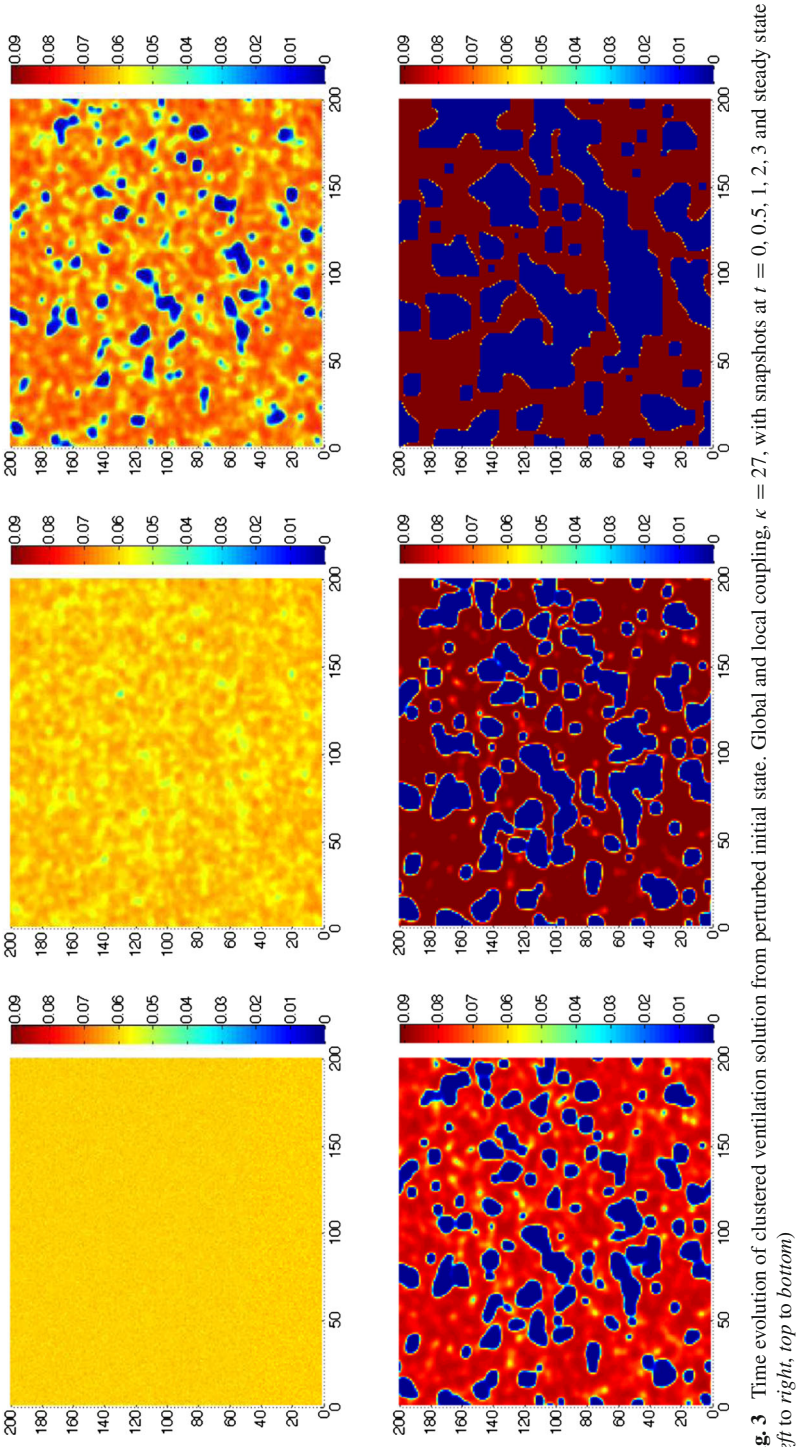

Fig. 3 Time evolution of clustered ventilation solution from perturbed initial state. Global and local coupling, $\kappa = 27$, with snapshots at $t = 0, 0.5, 1, 2, 3$ and steady state (*left* to *right*, *top* to *bottom*)

Several things are immediately obvious. First we can obtain an eigenvalue bound from Gershgorin's disk theorem:

$$\alpha - 4|\beta| \leq \lambda \leq \alpha + 4|\beta|$$

(where a real, symmetric matrix gives us real eigenvalues). Moreover one eigenvalue is obvious from inspection as the eigenvector $\mathbf{v} = [1, 1, 1, \ldots, 1]^\top$ has corresponding eigenvalue $\lambda = \alpha + 4\beta$. Thus if $\beta > 0$, the largest eigenvalue $\lambda_{max} = \alpha + 4\beta$ occurs on the boundary of the Gershgorin disk.

Moreover the full structure of the eigenvalues and eigenvectors is generally known because $\mathcal{J}$ is block circulant (or sometimes, compound circulant) (Tee 1963, 2007), and so

$$\lambda_{n,m} = \alpha + 2\beta(\cos(n\theta) + \cos(m\theta)), \quad \text{for } j, k = 1, \ldots, N$$

where $\theta = 2\pi/N$. This arises as a special case of the more general global coupling scenario, for which we give the full calculation in the next section. Thus independent of the sign of β the largest real eigenvalue approaches

$$\lambda_{max} \to \alpha + 4|\beta|$$

as N becomes large, either on or near the boundary of the Gershgorin disk depending on the parity of N and the sign of β.

However, because of the nature of the internal dynamics we cannot explicitly solve for the homogeneous fixed point which would allow explicit stability conditions. Nonetheless the block circulant structure of $\mathcal{J}$, and subsequent calculation of the eigenvalues and eigenvectors, allow much insight into the behaviour of the system.

3.2.2 Global coupling eigenvalues: general case

Here we consider the more general case of global coupling and show that the block circulant structure of the Jacobian is preserved. We need now to account for increases in driving pressure to counteract constriction and maintain total flow. That is,

$$P_b = P_b(r_k \, \forall k \in \mathcal{L}) = \hat{Q} \Big/ \left(\sum_{k \in \mathcal{L}} r_k^4(t) \right).$$

We define the contribution of this extra global coupling (as opposed to the previous local-only coupling) as $\gamma = \rho \frac{\partial \Phi}{\partial r_k}$ for $k \neq i, k \in \{\mathcal{L} \setminus \mathcal{N}_i\}$. Then the Jacobian matrix of the system will be the square matrix of order N^2 with the following structure

$$\mathcal{J} = \begin{bmatrix} A & B & C & \cdots & C & B \\ B & A & B & C & \cdots & C \\ C & B & A & B & C & \cdots \\ \vdots & & \ddots & \ddots & \ddots & \vdots \\ C & \cdots & C & B & A & B \\ B & C & \cdots & C & B & A \end{bmatrix}$$

with A, B and C being the square matrices of order N

$$A = \left.\begin{pmatrix} \alpha & \beta & \gamma & \cdots & \gamma & \beta \\ \beta & \alpha & \beta & \gamma & \cdots & \gamma \\ \gamma & \beta & \alpha & \beta & \gamma & \cdots \\ \vdots & & \ddots & \ddots & \ddots & \vdots \\ \gamma & \cdots & \gamma & \beta & \alpha & \beta \\ \beta & \gamma & \cdots & \gamma & \beta & \alpha \end{pmatrix}\right\} \mathrm{N}$$

$$B = \left.\begin{pmatrix} \beta & \gamma & & \cdots & & \gamma \\ \gamma & \beta & \gamma & \cdots & & \gamma \\ \vdots & & & \ddots & & \vdots \\ \gamma & & \cdots & & \gamma & \beta \end{pmatrix}\right\} \mathrm{N}, \text{ and } C = \left.\begin{pmatrix} \gamma & \cdots & & \cdots & \gamma \\ \vdots & \ddots & & & \vdots \\ \vdots & & & \ddots & \vdots \\ \gamma & \cdots & & \cdots & \gamma \end{pmatrix}\right\} \mathrm{N}.$$

As before, $\lambda = \alpha + 4\beta + (N^2 - 5)\gamma$ continues to be an eigenvalue associated with the eigenvector $[1, 1, 1, \ldots 1]^\top$. Similarly Gershgorin's theorem continues to bound the positive eigenvalues as

$$\lambda < \alpha + 4|\beta| + (N^2 - 5)|\gamma|$$

(though as a practical matter the positive bound is loose, as we shall see). Thus we will have to find the whole spectrum.

We can see that $\mathcal{J}$ is a block-circulant matrix and that the blocks A, B and C are themselves circulant matrices. Recall that the local-only coupling corresponds to the case $\gamma = 0$.

We begin by finding the eigenvalues and eigenvectors of the three circulant matrices. Let ρ be a scalar and let $\mathbf{w}$ be the vector

$$\mathbf{w} = \begin{bmatrix} 1 \\ \rho \\ \rho^2 \\ \vdots \\ \rho^{N-1} \end{bmatrix}.$$

If λ_A is the eigenvalue of A corresponding to $\mathbf{w}$, we obtain $A\mathbf{w} = \lambda_A \mathbf{w}$. and by substitution, the system

$$\begin{cases} \alpha + \beta(\rho + \rho^{N-1}) + \gamma(\rho^2 + \cdots + \rho^{N-2}) = \lambda_A \\ (\alpha + \beta(\rho + \rho^{-1}) + \gamma(\rho^2 + \cdots + \rho^{N-2}))\rho = \lambda_A \rho \\ \qquad\qquad\qquad\qquad\qquad\qquad \vdots \\ (\alpha + \beta(\rho^{-N+1} + \rho^{-1}) + \gamma(\rho^{-N+2} + \cdots + \rho^{-2}))\rho^{N-1} = \lambda_A \rho^{N-1}. \end{cases}$$

We take $\rho_n = e^{in\theta}$ where $\theta = \frac{2\pi}{N}$ and $n = 0, 1, \ldots, N-1$, so that $\rho^N = 1$ for all values of n. The system is then equivalent to the single equation

$$\alpha + \beta(\rho + \rho^{-1}) + \gamma(\rho^2 + \cdots + \rho^{N-2}) = \lambda_A$$

which gives us, if $r \neq 0$:

$$\begin{aligned} \lambda_{A,n} &= \alpha + 2\beta\cos(n\theta) + \gamma\rho^2(1 + \cdots + \rho^{N-4}) \\ &= \alpha + 2\beta\cos(n\theta) - \gamma(2\cos(n\theta) + 1) \end{aligned} \tag{8}$$

and if $n = 0$:

$$\lambda_{A,0} = \alpha + 2\beta + \gamma(N-3).$$

Each such $\lambda_{A,n}$ is an eigenvalue of A.

Furthermore, let $\mathbf{w}_n$ be the vector

$$\mathbf{w}_n = \begin{bmatrix} 1 \\ \rho_n \\ \rho_n^2 \\ \vdots \\ \rho_n^{N-1} \end{bmatrix}.$$

We have shown above that the N vectors $\mathbf{w}_n$ for $(n = 0, 1, \ldots, N-1)$ are eigenvectors. We can also see that these vectors are mutually orthogonal, as

$$\begin{aligned} \mathbf{w}_n^* \mathbf{w}_m &= [1, \bar{\rho_n}, \ldots, \bar{\rho_n}^{N-1}] \begin{bmatrix} 1 \\ \rho_m \\ \vdots \\ \rho_m^{N-1} \end{bmatrix} \\ &= 1 + e^{\frac{2\pi i(m-n)}{N}} + \cdots + e^{\frac{2\pi i(m-n)(N-1)}{N}} \\ &= \begin{cases} 0 & \text{if } n \neq m \\ N & \text{if } n = m \end{cases} \end{aligned}$$

and so the family of eigenvectors is orthogonal. We can apply the same process with B and C. As the order of these matrices is N too, we obtain the same eigenvectors $\mathbf{w}_n$.

A similar calculation gives the associated eigenvalues. If $n \neq 0$, then $B\mathbf{w}_n = \lambda_{B,n}\mathbf{w}_n$ gives us

$$\begin{aligned}\lambda_{B,n} &= \beta + \gamma(\rho + \cdots + \rho^{N-1}) \\ &= \beta + \gamma e^{i\pi n}\frac{\sin\left(\frac{N-1}{2}\theta n\right)}{\sin\left(\frac{\theta}{2}n\right)} \\ &= \beta - \gamma\end{aligned}$$

while if $n = 0$, the associated eigenvalue is $\lambda_{B,0} = \beta + (N-1)\gamma$. Similarly for the matrix C, if $n \neq 0$, $\lambda_{C,n} = 0$ and $\lambda_{C,0} = N\gamma$.

We can now apply this process to the matrix $\mathcal{J}$, by considering the compound vectors

$$W_{n,m} = \begin{bmatrix} \mathbf{w}_n \\ \rho_m \mathbf{w}_n \\ \rho_m^2 \mathbf{w}_n \\ \vdots \\ \rho_m^{N-1}\mathbf{w}_n \end{bmatrix}$$

with $\mathbf{w}_n$ as before. Given that $\mathbf{w}_n$ are the eigenvectors of the three matrices A, B and C, then $W_{n,m}$ is an eigenvector of $\mathcal{J}$. Let $\lambda_{n,m}$ be the eigenvalue associated with $W_{n,m}$. Then $\mathcal{J}W_{n,m} = \lambda_{n,m}W_{n,m}$ gives us the single equation (as $\rho_m^N = 1$)

$$Aw_n + (\rho_m + \rho_m^{-1})Bw_n + (\rho_m^2 + \cdots \rho_m^{N-2})Cw_n = \lambda_{n,m}W_{n,m}$$

and so gives us the eigenvalues. If $m \neq 0$,

$$\lambda_{n,m} = \lambda_{A,n} + 2\cos(m\theta)\lambda_{B,n} - \lambda_{C,n}(2\cos(m\theta) + 1)$$

and if $m = 0$,

$$\lambda_{n,0} = \lambda_{A,n} + 2\lambda_{B,n} + (N-3)\lambda_{C,n}.$$

By substitution of the values of λ_A, λ_B and λ_C, the eigenvalues of the matrix $\mathcal{J}$ are given by

$$\lambda_{n,m} = \alpha + 2\beta(\cos(n\theta) + \cos(m\theta)) - \gamma(2\cos(n\theta) + 2\cos(m\theta) + 1)$$

if $(n, m) \neq (0, 0)$, and

$$\lambda_{0,0} = \alpha + 4\beta + (N^2 - 5)\gamma.$$

These results, obtained for the local and global coupling system, can be thought of as a generalization of the local-coupling only system, with the sub-case given when $\gamma = 0$. We find then

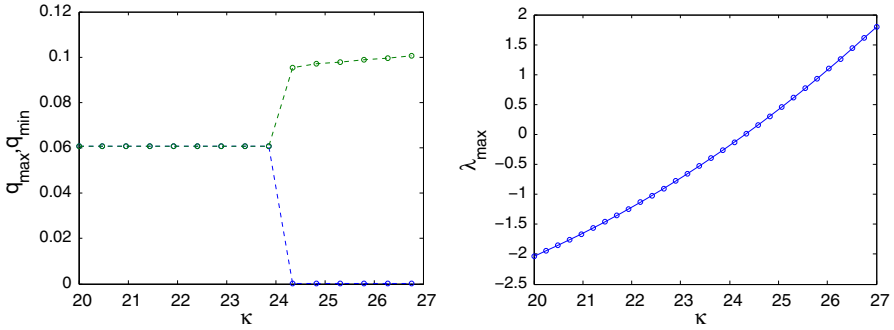

Fig. 4 Global and local coupling bifurcation to clustered solutions ($N = 8$). *Left panel* max and min local flow in each terminal unit. *Right panel* corresponding λ_{max}

$$\lambda_{n,m} = \alpha + 2\beta(\cos(n\theta) + \cos(m\theta))$$

as before.

3.3 Global coupling leads to clustered ventilation defects

Understanding the structure of the eigenvalues and eigenvectors of the system allows us to understand the loss of stability of the homogeneous solution into clustered ventilation defects (Fig. 3). Even though we cannot write α, β and γ explicitly in terms of the system parameters (because we cannot write the homogeneous equilibrium explicitly because of the nature of the nonlinearities), we can understand how the homogeneous solution loses stability.

We argue from physical intuition (and numerical evidence) that

$$\beta > 0, \text{ and}$$
$$\gamma \leq 0$$

within the physiological range, with important exceptions to be discussed. Thus as the lattice becomes large, the largest eigenvalue tends to $\lambda = \alpha + 4\beta - 5\gamma$ and when this largest eigenvalue crosses the axis the homogeneous solution loses stability (see Fig. 4) and clustered ventilation solutions emerge—see Fig. 3.

Of course this only demonstrates numerically that clusters emerge. To understand why, analytically, we must look at the eigenvectors of the system.

3.4 Eigenvector associated with the largest eigenvalue

3.4.1 Local-only coupling

In the case of local-only coupling, we consider two cases: $\beta > 0$ and $\beta < 0$. (In the $\beta = 0$ case the lattice is uncoupled).

We argued previously that from physical intuition we expect $\beta > 0$ within the physiological range. In this case, the largest eigenvalue is $\lambda = \alpha + 4\beta$ and is associated with the eigenvector $[1, 1, 1, \ldots 1]^\top$.

The $\beta < 0$ case turns out to be an important exception. Here we can see that the eigenvalues are all in the disk of center α and radius $4|\beta|$ (Gershgorin disk) and that, when N becomes large, the largest eigenvalue tends to $\alpha - 4\beta$. This eigenvalue is obtained for $n = m = [\frac{N}{2}]$, which means that the eigenvector associated with the largest eigenvalue tends to

$$W = \begin{bmatrix} \mathbf{w} \\ -\mathbf{w} \\ \mathbf{w} \\ \vdots \\ (-1)^{N-1}\mathbf{w} \end{bmatrix}$$

with

$$\mathbf{w} = \begin{bmatrix} 1 \\ -1 \\ 1 \\ \vdots \\ (-1)^{N-1} \end{bmatrix}$$

which corresponds to a "checkerboard" vector. Thus if the local-only coupling system has the largest eigenvalue cross the stability boundary when $\beta < 0$ we expect a checkerboard pattern to emerge, though the physiological relevance of this solution would be in doubt.

3.4.2 Global and local coupling

In the case of local and global coupling, when $\beta > 0$ and $\gamma < 0$, the largest eigenvalue is obtained when (n, m) is one of the four couples : $(1, 0)$, $(N - 1, 0)$, $(0, 1)$ or $(0, N - 1)$. In these cases, $\lambda = \alpha + 2\beta(1 + \cos(\theta)) - \gamma(2\cos(\theta) + 3)$ and tends to

$$\lambda_\infty = \alpha + 4\beta - 5\gamma$$

as N becomes large. Given the previous results, the multiplicity of λ is 4 and we know four complex orthogonal eigenvectors associated with this eigenvalue : $W_1 = W_{1,0}$, $W_2 = W_{N-1,0}$, $W_3 = W_{0,1}$, $W_2 = W_{0,N-1}$. We can see that we can obtain four real orthogonal eigenvectors associated to the same eigenvalue, by considering

$$V_1 = \frac{1}{2}(W_1 + W_2), \quad V_2 = \frac{1}{2i}(W_1 - W_2),$$
$$V_3 = \frac{1}{2}(W_3 + W_4), \quad V_4 = \frac{1}{2i}(W_3 - W_4).$$

Here we have used here the fact that $\rho_{N-1}^k + \rho^k$ is a real number and $\rho_{N-1}^k - \rho^k$ is an imaginary number, for every integer k. The new family of vectors is orthogonal because the original vectors were orthogonal and had the same norm. Thus we obtain

$$V_1 = \begin{bmatrix} 1 \\ \vdots \\ 1 \\ \cos(\theta) \\ \vdots \\ \cos(\theta) \\ \cos(2\theta) \\ \vdots \\ \cos((N-1)\theta) \\ \vdots \\ \cos((N-1)\theta) \end{bmatrix} \begin{matrix} \\ \\ \\ \\ \\ \\ \\ \\ \\ \\ \end{matrix} \begin{matrix} \\ \\ \} \text{N} \\ \\ \\ \\ \\ \\ \\ \\ \end{matrix} \qquad V_2 = \begin{bmatrix} 0 \\ \vdots \\ 0 \\ \sin(\theta) \\ \vdots \\ \sin(\theta) \\ \sin(2\theta) \\ \vdots \\ \sin((N-1)\theta) \\ \vdots \\ \sin((N-1)\theta) \end{bmatrix} \begin{matrix} \\ \\ \} \text{N} \\ \\ \\ \\ \\ \\ \\ \\ \end{matrix}$$

$$V_3 = \begin{bmatrix} 1 \\ \cos(\theta) \\ \vdots \\ \cos((N-1)\theta) \\ 1 \\ \cos(\theta) \\ \vdots \\ 1 \\ \cos(\theta) \\ \vdots \\ \cos((N-1)\theta) \end{bmatrix} \begin{matrix} \\ \\ \\ \} \text{N} \\ \\ \\ \\ \\ \\ \\ \\ \end{matrix} \qquad V_4 = \begin{bmatrix} 0 \\ \sin(\theta) \\ \vdots \\ \sin((N-1)\theta) \\ 1 \\ \sin(\theta) \\ \vdots \\ 1 \\ \sin(\theta) \\ \vdots \\ \sin((N-1)\theta) \end{bmatrix} \begin{matrix} \\ \\ \\ \} \text{N} \\ \\ \\ \\ \\ \\ \\ \\ \end{matrix} .$$

These vectors of order N^2 can be seen in the lattice as $N \times N$ matrices. In fact if we consider the associated matrix of each vector, we can see that:

$$V_1(x, y) = \cos(x\theta) \tag{9}$$
$$V_2(x, y) = \sin(x\theta) \tag{10}$$
$$V_3(x, y) = \cos(y\theta) \tag{11}$$
$$V_4(x, y) = \sin(y\theta) \tag{12}$$

with x and y being the coordinate of the point in the lattice, both varying from 0 to $N - 1$. Direct numerical calculation of the eigenspace for the largest eigenvalue is in good agreement, illustrating these 'long-wave' modes: see Fig. 5. These four eigenvectors are all N-periodic (along the x or y axis), and this 'long wave' will tend to gather closed airways together.

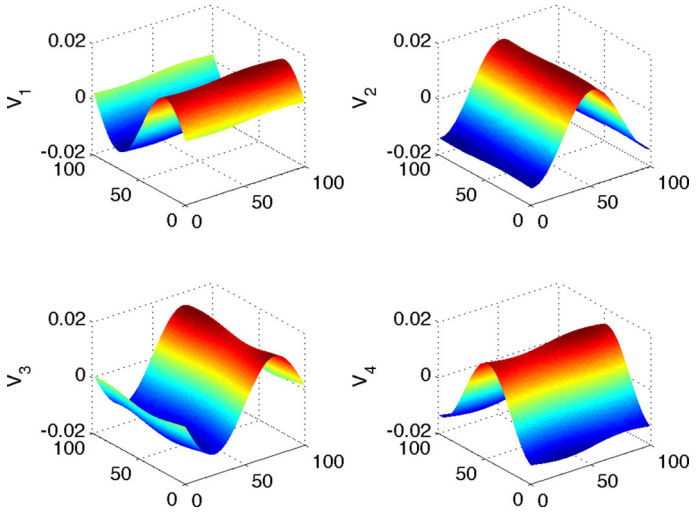

Fig. 5 Global and local coupling—eigenvectors associated with $\lambda_{\max}$. Direct numerical calculation of the eigenvectors and eigenvalues also shows the predicted 'long-wave' modes associated with the largest eigenvalue. Note that the basis of the eigenspace found numerically differs (approximately, and arbitrarily) from the analytic calculation by: $V_1 \mapsto V_4$, $V_2 \mapsto V_1$, $V_3 \mapsto V_2$, $V_4 \mapsto V_3$. (c.f. Eqs. 9–12)

Interestingly, as we shall see, other positive eigenvalues follow the largest very near the bifurcation point, and these play an important role. Thus we have to take into account all positive eigenvalues which are responsible of the instability of the system.We can see that $W_{n,m}$ and $W_{N-n,N-m}$ are eigenvectors associated to the same eigenvalue $\lambda_{n,m}$. As their roles are symmetric, we will now consider that n is smaller than $N-n$, and m smaller than $N-m$. By using the same process as above, we can add them to obtain a real eigenvector:

$$V_{n,m} = W_{n,m} + W_{N-n,N-m} = \begin{bmatrix} 1 \\ \rho_n \\ \vdots \\ \rho_n^{N-1} \\ \rho_m \\ \rho_m \rho_n \\ \vdots \\ \rho_m \rho_n^{N-1} \\ \vdots \\ \rho_m^{N-1} \rho_n^{N-1} \end{bmatrix} + \begin{bmatrix} 1 \\ \rho_{N-n} \\ \vdots \\ \rho_{N-n}^{N-1} \\ \rho_{N-m} \\ \rho_{N-m} \rho_{N-n} \\ \vdots \\ \rho_{N-m} \rho_{N-n}^{N-1} \\ \vdots \\ \rho_{N-m}^{N-1} \rho_{N-n}^{N-1} \end{bmatrix}$$

$$= 2 \begin{bmatrix} 1 \\ \cos(n\theta) \\ \vdots \\ \cos(n(N-1)\theta) \\ \cos(m\theta) \\ \cos((m+n)\theta) \\ \vdots \\ \cos((m+(N-1)n)\theta) \\ \vdots \\ \cos(((N-1)m+(N-1)n)\theta) \end{bmatrix}$$

If we again consider this vector as a $N \times N$ matrix on the lattice, we obtain

$$V_{n,m}(x, y) = \cos((nx + my)\theta)$$

so the eigenvector will be $\frac{N}{n}$-periodic along the x-axis and $\frac{N}{m}$-periodic along the y-axis. For example, the second largest eigenvalue is obtained for $(n, m) = (1, 1)$ (and three other symmetric values), which means that the eigenvector is N periodic along the x **and** the y axes. This means that the biggest clustered region is obtained when the largest eigenvalue is the only positive eigenvalue, and that clustered regions will be smaller and smaller when there are more positive eigenvalues. We can even have an idea of the size of the clustered region: $\frac{N}{2n}$ along the x-axis and $\frac{N}{2m}$ along the y-axis, where (n, m) is one of the couple associated to the smallest positive eigenvalue (we still consider $n \leq N - n$ and $m \leq N - m$).

3.5 Unstable modes and cluster size

Given the structure of the eigenvalues and eigenvectors, we expect that the characteristic length of the clustered ventilation defects is determined by the number of positive eigenvalues, with each additional eigenvalue adding a family of unstable modes with higher and higher frequencies within the lattice. Numerically we see exactly the result expected from the theory, illustrated by advancing well past the bifurcation in κ (Fig. 4) studied already. Recall that the eigenvalues are given in this case by Eq. 8. In Fig. 6 we illustrate the characteristic cluster sizes at steady state, first for a value very near the first crossing with only long-wave modes (from the largest eigenvalue only), and subsequently for increased values of κ pushing more and more high frequency modes across the stability boundary.

3.6 Local-only coupling does not admit clustered ventilation solutions

If we employ local-only coupling in the physiological range of parameter space considered for the local and global coupling case, the homogeneous solution remains stable. However efforts to demonstrate that the homogeneous solution is always stable

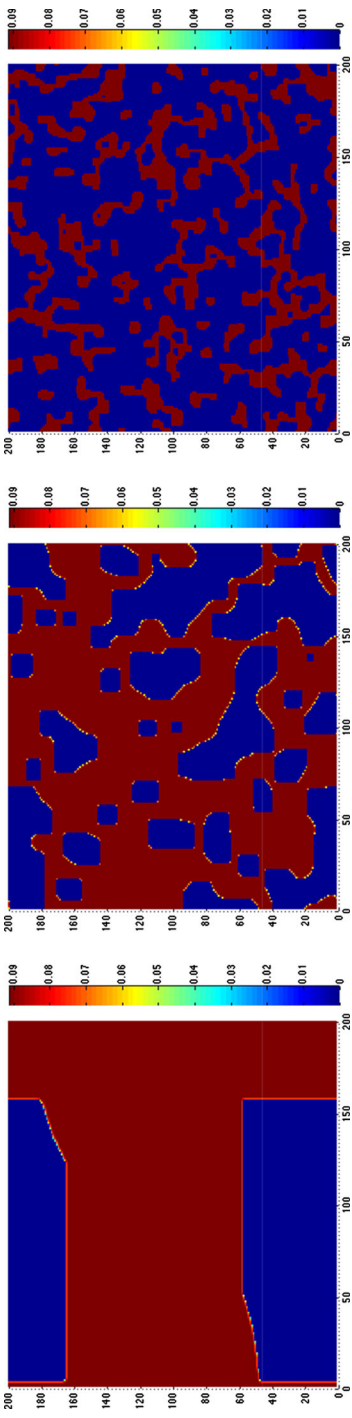

Fig. 6 Cluster size dependence, 200×200 square lattice. As more eigenvalues cross the axis, higher and higher frequency modes contribute to the clustered solutions, as predicted. Here $\kappa = 23.3, 26, 50$ from *left* to *right* (global and local coupling case)

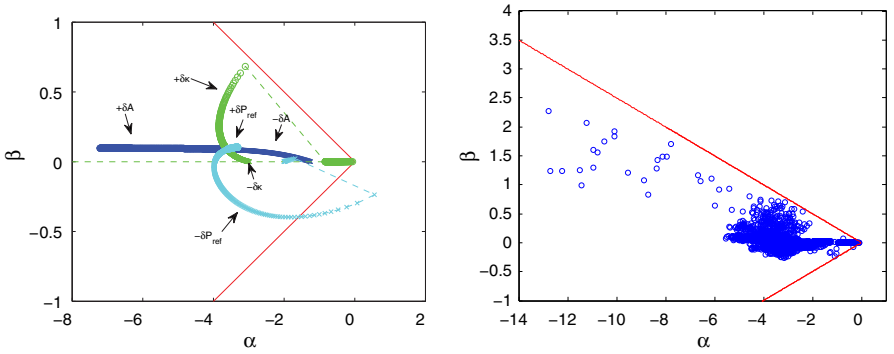

Fig. 7 Local-only coupling and stability. The *red lines* indicate the stability boundary. Solutions which cross the boundary for $\beta > 0$ may result in clustered solutions, while those which cross for $\beta < 0$ generate checkerboards. *Left panel* parameter family branches, with the $-\delta P_{ref}$ branch leading to checkerboard solutions. *Right panel* MCMC search for region of parameter space which may produce clustered solutions (100,000 trials) (color figure online)

in this case in fact turned up a counter example. Consider in Fig. 7, left panel, the effects of each parameter on the values of α and β. We already know that independent of the sign of β we have the stability condition $\alpha + 4|\beta| < 0$ and so by looking at the (α, β) plane we can easily draw the stability boundary. The initial parameter values begin well away from the boundary, but naive exploration of parameter space by varying parameters independently reveals that in fact the $-\delta P_{ref}$ branch crosses the stability boundary (just before P_{ref} becomes negative). Examining this case more closely we find that this is in the exception case where $\beta < 0$, meaning that physical intuition about the role of nearest-neighbour coupling has now reversed and that as a result the checkerboard is the first unstable mode.

Caution must be exercised in physiological interpretation; both the very small value of P_{ref} and the fact that this is the exception case where β has changed sign both indicate that this may be an anomaly outside of the physiological range. (Here the reference state is at such low pressure that the time course of the airways is not constricting but expanding; the tethering force, relative to reference, is then not an expanding force but a compressing force, hence the change in the sign of β. In short the design of the model has been reversed.) Nonetheless it is interesting that the local-coupling only system does not always have a stable homogeneous solution, and that the heterogeneous solutions which emerges is qualitatively different.

While the naive exploration revealed only occurrences of the $\beta < 0$ instability, it remains possible that there is a region of parameter space which allows $\beta > 0$ instabilities. To explore this possibility we conducted a series of Markov Chain Monte Carlo (MCMC) searches of parameter space, optimized toward the line $\alpha = -4\beta$; 100,000 trials failed to turn up any such instabilities (see Fig. 7, right panel). Of course this does not preclude there being regions which we have not been able to find, but it suggests at least that any such region of parameter space is small. If this were the case, the $\lambda_{max} = \alpha + 4\beta$ would be associated with the $[1, 1, 1, \ldots 1]^\top$ eigenvector and thus the homogeneous solution would be preserved if this is the only positive eigenvalue.

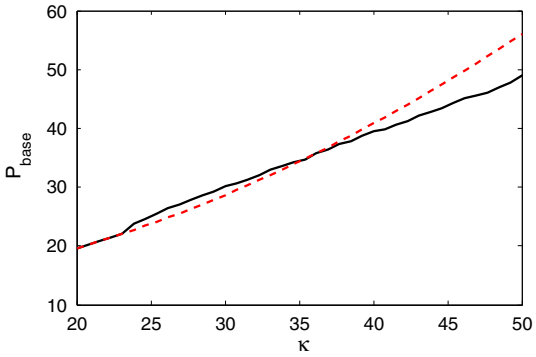

Fig. 8 Relative efficiency of homogeneous and heterogeneous states. Driving pressures required to maintain homogeneous and clustered solutions in global and local coupling case. (homogeneous–*red, dashed*; clustered—*black, solid*) (color figure online)

Only if the second largest eigenvalue also crossed the axis would the long-wave modes become unstable, potentially leading to clustered ventilation solutions.

3.7 Efficiency of stabilized homogeneous solution

One question which naturally arises is whether stabilizing the homogeneous solution to prevent clustered ventilation defects would be beneficial. That is, if clustered VDs are a hallmark of asthma, and they can be eliminated, does that improve respiratory function in and of itself? Or are clustered VDs merely a by-product, or even a beneficial response, to the underlying airway constriction?

While this is an impossible experiment to conduct on patients, it is trivial to "stabilize" the homogeneous solution by exploiting the numerical meta-stability (that is, do not perturb the uniform solution). Then a direct comparison can be made between the respiratory efficiency of the homogeneous, and clustered, solutions. One obvious measure is the differential in driving pressure required to maintain flow, given in Fig. 8. In fact the difference is relatively small, though initially the heterogeneous solution does in fact require greater driving pressures than a homogeneous solution would, if it were stable. However the effect is reversed for more severe constriction, with the clustered solution becoming more efficient. Because of the connection with cluster size, this suggests that large clusters are relatively inefficient while smaller clusters may in fact be more efficient than the homogeneous solution.

That said, the effect is small, and this is only one simple way of considering the wider merits of homogeneous versus heterogeneous solutions. Other considerations, such as epithelial damage from airway reopening (e.g. Kay et al. 2004; Bilek et al. 2003; Yalcin at al. 2007) or ventilation/perfusion (V/Q) matching (Wagner et al. 1987; Rodriguez-Roisin et al. 1991), might be considered more important.

3.8 Alternate airway models

One challenge in the analysis of this model is the inability to write the homogeneous equilibrium explicitly (that is, even for a single airway, coupling considerations

aside).This naturally arises in part from the complexity of the Lambert model (Lambert et al. 1982) for the airway wall, Eq. 2, giving luminal radius as a function of transmural pressure. This piecewise function employs two rectangular hyperbolae matched at zero transmural pressure for continuity. Naturally one might consider if a simpler model might be available which would preserve the qualitative features of the full model but allowing greater analysis, particularly an explicit solution for the fixed points. Two possibilities arise: the model of Thorpe and Bates (1997), and a linear pressure-radius relationship (possibly with parameters extracted from tangency with the one of the nonlinear models). As it turns out, both simplifications do admit clustered ventilation defects (so long as negative radii are excluded), and thus the nonlinearity of the Lambert model is not critical to this central result; however, neither does this allow the sought analytic simplification. That is, even with a linear R–P relationship the fixed points are roots of a sixth-order polynomial, arising from the combination of the r^{-4} dependence in Eq. 7 and the r^2 dependence of Eq. 4 combined into Eq. 3. Thus the complexity of the airway wall model itself is neither critical for the qualitative behaviour of clustered VDs, nor solely responsible for the analytic challenges.

4 Hexagonal and cubic lattice extensions

To this point we have considered only the case of 2D square lattice coupling. One might naturally wonder what role the geometry of this assumption plays; here we consider (2D) hexagonal and (3D) cubic lattice extensions. We alter the model as follows, changing Eq. 5 to

$$2\mu_h(r_i; r_{j_1}, \ldots, r_{j_6}) = P_b \frac{A}{7}\left(r_i^4 + \sum_{j\in\mathcal{N}_i} r_j^4\right) \tag{13}$$

where now $\mathcal{N}_i$ contains 6 neighbouring sites. The normalizing coefficient has been changed so that the homogeneous fixed points remain unchanged. However, this does alter the values of α, β and γ so that we now have

$$\begin{aligned}
\alpha_h &= \rho\left(\frac{\partial \Phi_h}{\partial r_i}(\mathbf{r}^*) - 1\right)\\
\beta_h &= \rho\frac{\partial \Phi_h}{\partial r_j}(\mathbf{r}^*)\\
\gamma_h &= \rho\frac{\partial \Phi_h}{\partial r_k}(\mathbf{r}^*)
\end{aligned}$$

for $j \in \mathcal{N}_i$ and $k \in \{\mathcal{L} \setminus \mathcal{N}_i\}$, $k \neq i$ at the homogeneous fixed point $\mathbf{r}^* = [r^*, r^*, \ldots, r^*]$, where we use the subscript h to distinguish the hexagonal and cubic lattice cases from the previous square lattice.

4.1 Hexagonal lattice

In this section, we only consider lattices of order N, with N being an even number, in order to obtain a whole hexagonal lattice.

4.1.1 Eigenvalues of the Jacobian

In the hexagonal case, each airways has six coupled neighbours. The Jacobian matrix for the system thus has the following structure

$$\mathcal{J}_h = \begin{bmatrix} A_h & B_h & C_h & \cdots & C_h & B_h \\ B_h' & A_h & B_h' & C_h & \cdots & C_h \\ C_h & B_h & A_h & B_h & & \vdots \\ \vdots & & \ddots & \ddots & \ddots & C_h \\ C_h & \cdots & C_h & B_h & A_h & B_h \\ B_h' & C_h & \cdots & C_h & B_h' & A_h \end{bmatrix}$$

with B_h' being the transpose of B_h. Now A_h and C_h are the same square matrices of order N as before but now with α_h and γ_h, and B_h is given by

$$B_h = \left.\begin{pmatrix} \beta_h & \gamma_h & \cdots & \gamma_h & \beta_h \\ \beta_h & \beta_h & \gamma_h & \cdots & \gamma_h \\ \gamma_h & \beta_h & \beta_h & & \vdots \\ \vdots & & \ddots & \ddots & \gamma_h \\ \gamma_h & \cdots & \gamma_h & \beta_h & \beta_h \end{pmatrix}\right\} \mathrm{N}$$

The main difference between the square lattice and this one is the matrix B_h, which now has a sub-diagonal row. Thus B_h is no longer symmetric, and so $\mathcal{J}_h$ is not block-circulant. Still, the previous process can be modified in order to find the eigenvalues of the system.

We already know the eigenvalues and eigenvectors of A_h and C_h. The matrix B_h remains circulant, so we already know its eigenvectors ($\mathbf{w}_r$) and the associated eigenvalues are

$$\begin{aligned} \lambda_{B,n} &= \beta_h(1 + \rho_n^{-1}) + \gamma_h(\rho_n \cdots \rho_n^{N-2}) \\ &= \beta_h(1 + \rho_n^{-1}) + 2\gamma_h \rho_n^{-1/2} \cos\left(\frac{n\theta}{2}\right) \\ &= \rho_n^{-1/2} \cos\left(\frac{n\theta}{2}\right)(2\beta_h - 2\gamma_h) \end{aligned}$$

for $n \neq 0$ and $\lambda_{B,0} = 2\beta_h + (N-2)\gamma_h$ if $n = 0$.

The matrix B_h' has the same eigenvalues as B_h but the eigenvector associated with the eigenvalue $\lambda_{B,n}$ is not $\mathbf{w}_n$ but $\mathbf{w}_{N-n}$, and we can easily see that $\lambda_{B,N-n} = \overline{\lambda_{B,n}}$.

$\mathcal{J}_h$ is not block circulant because of the transpose of B_h, so we make the ansatz that $W_{n,m}$ is

$$W_{n,m} = \begin{bmatrix} a_n \mathbf{w}_n \\ a_n^{-1} \rho_m \mathbf{w}_n \\ a_n \rho_m^2 \mathbf{w}_n \\ \vdots \\ a_n^{-1} \rho_m^{N-1} \mathbf{w}_n \end{bmatrix}$$

for some a_n. If $n = 0$ or $n = \frac{N}{2}$, $\lambda_{B,n}$ is real, so we can take $a_n = 1$ and we obtain a single relation for $\lambda_{n,m}$. If $n \neq 0$ and $n \neq \frac{N}{2}$, $C\mathbf{w}_n = 0$ and thus, $W_{n,m}$ is an eigenvector of M if $\lambda_{n,m}$ satisfies

$$\begin{cases} \lambda_{A,n} + a_n^{-2} \lambda_{B,n} (\rho_m + \rho_m^{-1}) = \lambda_{n,m} \\ \lambda_{A,n} + a_n^{2} \overline{\lambda_{B,n}} (\rho_m + \rho_m^{-1}) = \lambda_{n,m} \end{cases}$$

and we choose $a_n = \left(\frac{\lambda_{B,n}}{|\lambda_{B,n}|} \right)^{1/2}$ so that we obtain a single relation. Given the value of $\lambda_{B,n}$, we obtain

$$a_n = \begin{cases} \rho_n^{-1/4} & \text{if } 0 < n < \frac{N}{2} \\ i\rho_n^{-1/4} & \text{if } \frac{N}{2} < n < N \\ 1 & \text{if } n = 0 \text{ or } n = \frac{N}{2} \end{cases}$$

and thus

$$\lambda_{n,m} = \begin{cases} \lambda_{A,n} + 2|\lambda_{B,n}| + (N-3)\lambda_{C,n}, & \text{if } m = 0 \\ \lambda_{A,n} + 2|\lambda_{B,n}| \cos(m\theta) - \lambda_{C,n}(2\cos(m\theta) + 1), & \text{for } m \neq 0. \end{cases}$$

By substitution, we finally obtain N^2 eigenvalues

$$\lambda_{n,m} = \begin{cases} \alpha_h + 6\beta_h + (N^2 - 7)\gamma_h, & \text{if } n = m = 0 \\ \alpha_h + 2\beta_h (\cos(n\theta) + 2|\cos(n\theta/2)|\cos(m\theta)) & \\ \quad -\gamma_h (2\cos(n\theta) + 4|\cos(n\theta/2)|\cos(m\theta) + 1), & \text{otherwise,} \end{cases}$$

where $n = 0, 1, \ldots, N-1$ and $m = 0, 1, \ldots, N-1$.

4.1.2 Eigenvector associated with the largest eigenvalue

When $\beta_h > 0$ and $\gamma_h < 0$, the largest eigenvalue is obtained for the couples $(n, m) = (1, 0)$ and $(n, m) = (N-1, 0)$. As $a_1 = \rho_1^{-1/4}$ and $a_{N-1} = i\rho_{N-1}^{-1/4} = \rho_1^{1/4}$, the two corresponding eigenvectors are

$$W_{1,0} = \begin{bmatrix} \rho_1^{-1/4}\mathbf{w}_1 \\ \rho_1^{1/4}\mathbf{w}_1 \\ \rho_1^{-1/4}\mathbf{w}_1 \\ \vdots \\ \rho_1^{1/4}\mathbf{w}_1 \end{bmatrix} \text{ and } W_{N-1,0} = \begin{bmatrix} \rho_1^{1/4}\mathbf{w}_{N-1} \\ \rho_1^{-1/4}\mathbf{w}_{N-1} \\ \rho_1^{1/4}\mathbf{w}_{N-1} \\ \vdots \\ \rho_1^{-1/4}\mathbf{w}_{N-1} \end{bmatrix}.$$

Here again, we can obtain real eigenvectors by considering

$$V_1 = \tfrac{1}{2}\left(W_{1,0} + W_{N-1,0}\right) = \begin{bmatrix} \cos(\frac{-\theta}{4}) \\ \cos(\frac{3\theta}{4}) \\ \vdots \\ \cos((N-1)\theta - \frac{\theta}{4}) \\ \cos(\frac{\theta}{4}) \\ \cos(\frac{5\theta}{4}) \\ \vdots \\ \cos((N-1)\theta + \frac{\theta}{4}) \\ \cos(\frac{-\theta}{4}) \\ \vdots \\ \cos((N-1)\theta - \frac{\theta}{4}) \\ \vdots \\ \cos(\frac{\theta}{4}) \\ \vdots \\ \cos((N-1)\theta + \frac{\theta}{4}) \end{bmatrix} \left.\begin{matrix} \\ \\ \\ \\ \\ \\ \\ \\ \\ \\ \\ \\ \\ \\ \end{matrix}\right\} \text{N} \tag{14}$$

and $V_2 = \frac{1}{2i}\left(W_{1,0} - W_{N-1,0}\right)$ which is the same vector with sine instead of cosine. If we interpret these vectors on the $N \times N$ lattice, we can see that

$$V_1(x, y) = \cos(x\theta + (-1)^{y-1}\theta/4)$$
$$V_2(x, y) = \sin(x\theta + (-1)^{y-1}\theta/4)$$

with $x, y \in [0, (N-1)]$. As N becomes large, $\frac{\theta}{4} \to 0$, and the two eigenvectors will tend to be N-periodic. Similarly, the eigenvectors associated with the next largest eigenvalues introduce higher frequency modes.

4.1.3 Local-only coupling case

We will now focus on the particular case $\gamma_h = 0$, corresponding to local only coupling.
$\beta_h > 0$ case

When $\beta_h > 0$, which is the 'physical' case, the largest eigenvalue is $\alpha_h + 6\beta_h$ and the associated eigenvector is the homogeneous one. But the second largest eigenvalue corresponds to the 'longwave' eigenvectors (as in Sect. 4.1.2) and the eigenvalue tends to $\alpha_h + 6\beta_h$ as N becomes large. The natural question then is if this instability can be realized, as in the square lattice case. In both square and hexagonal lattices, we know that

$$\begin{aligned}\alpha/\rho &= \frac{\partial\phi}{\partial r_i}(\mathbf{r}^*) \\ &= \frac{\partial R}{\partial P}(P(\mathbf{r}^*))\frac{\partial P}{\partial r_i}(\mathbf{r}^*) - 1 \\ &= \frac{\partial R}{\partial P}(P(\mathbf{r}^*))\left(\frac{\partial}{\partial r_i}\frac{-\kappa R_{ref}}{r_i} + \frac{\partial\mu}{\partial r_i}(\mathbf{r}^*)g(r^*) + \mu\frac{\partial g}{\partial r_i}(r^*)\right) - 1\end{aligned}$$

and

$$\begin{aligned}\beta/\rho &= \frac{\partial\phi}{\partial r_j}(\mathbf{r}^*) \\ &= \frac{\partial R}{\partial P}(P(\mathbf{r}^*))\left(\frac{\partial\mu}{\partial r_j}(\mathbf{r}^*)g(r^*)\right).\end{aligned}$$

where $g(r) = 2((\frac{R_{ref}-r}{R_{ref}}) + 1.5(\frac{R_{ref}-r}{R_{ref}})^2)$.

However, in the hexagonal lattice case

$$\frac{\partial\mu_h}{\partial r_i}(\mathbf{r}^*) = \frac{\partial\mu_h}{\partial r_j}(\mathbf{r}^*) = \frac{4}{7}P_b A(r^*)^3$$

and in the square lattice case

$$\frac{\partial\mu}{\partial r_i}(\mathbf{r}^*) = \frac{\partial\mu}{\partial r_j}(\mathbf{r}^*) = \frac{4}{5}P_b A(r^*)^3$$

and all the other values are the same. We obtain then $\beta_h = \frac{5}{7}\beta$ and $\alpha_h = \alpha - \frac{2}{7}\beta$ which gives us finally

$$\alpha_h + 6\beta_h = \alpha + 4\beta.$$

Thus when $\beta > 0$, the largest eigenvalue in the square lattice case is the same as in the hexagonal lattice case. Thus if this instability does not occur in the square lattice model (as the numerical evidence suggests, see Sect. 3.6), neither does it occur in the hexagonal lattice.

$\beta < 0$ *case*:

In this aphysical case, we saw previously that we could obtain a checkerboard system for the square lattice. With the hexagonal formulation, the largest eigenvalue is be obtained when $n = \frac{N}{3}$ (or $n = \frac{2N}{3}$) and $m = \frac{N}{2}$, and thus $\lambda_{max} = \alpha - 3\beta$. We assume here that N is a multiple of 3. This eigenvalue is multiplicity two and the basis of the eigenspace is given by

$$V_1 = \begin{matrix} 1 & 0 & -1 & \cdots & 1 & 0 & -1 \\ -1 & 1 & 0 & \cdots & -1 & 1 & 0 \\ & & & \vdots & \vdots & & \\ 1 & 0 & -1 & \cdots & 1 & 0 & -1 \\ -1 & 1 & 0 & \cdots & -1 & 1 & 0 \end{matrix}$$

and

$$V_2 = \begin{matrix} -1 & 2 & -1 & \cdots & -1 & 2 & -1 \\ -1 & 2 & -1 & \cdots & -1 & 2 & -1 \\ & & & \vdots & \vdots & & \\ -1 & 2 & -1 & \cdots & -1 & 2 & -1 \\ -1 & 2 & -1 & \cdots & -1 & 2 & -1 \end{matrix}$$

4.2 Numerical results

As in the square lattice case, there is a shortwave instability corresponding to the aphysical $\beta < 0$ case, with eigenvalues and eigenvectors as computed in Sect. 4.1.3. Numerical simulations for this case are given in Fig. 9, with the steady state solution in the left panel (normalized flow), and the basis for the eigenspace corresponding to the largest eigenvalue in the center and right panels. Here there is a qualitative difference with the square lattice, as the stable pattern (and unstable modes) can no longer be described as checkerboard patterns.

In the physically realistic $\beta > 0$ case with the global and local coupling, clustered VDs emerge in a similar fashion to the square lattice mechanism, via long-wave unstable modes. As more and more eigenvalues cross the axis, higher frequency modes occur and lead to decreased characteristic length scale for the ventilation defects. We give simulation examples of this dependence in Fig. 10, where here the mechanism is qualitatively similar to the square lattice case.

4.3 Cubic lattice

The cubic lattice case can be understood as a hybrid of the square and hexagonal lattice cases. The partial derivatives remain the same as in the hexagonal case, with stability boundary $\alpha_c + 6|\beta_c| = \alpha + 4|\beta|$. The Jacobian remains block circulant, now of order N^3. In the $\beta < 0$ case, there is an aphysical local-only stability loss into a

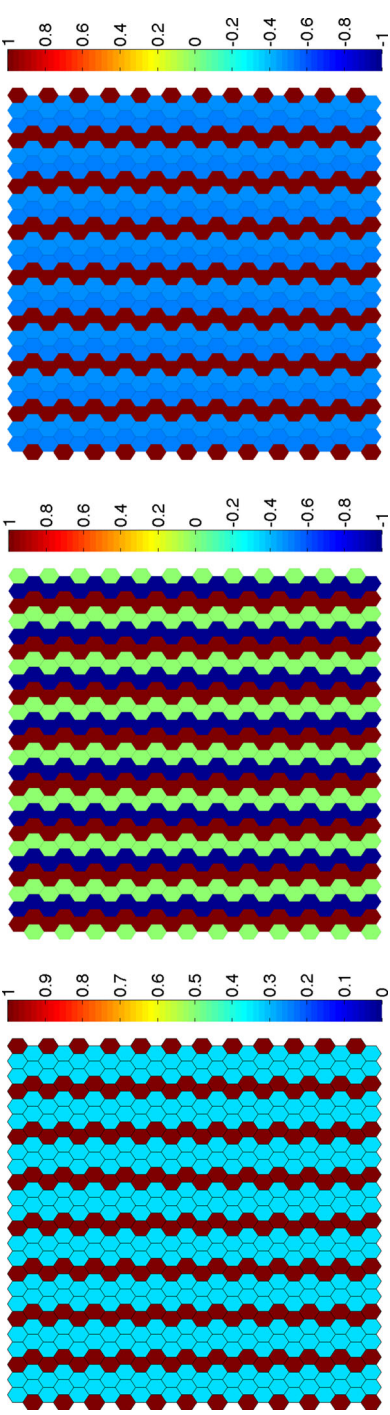

Fig. 9 Local only coupling, hexagonal lattice, $\beta < 0$ instability. *Left panel* steady state flow, normalized. *Right* and *center panels* basis of eigenspace for largest eigenvalue

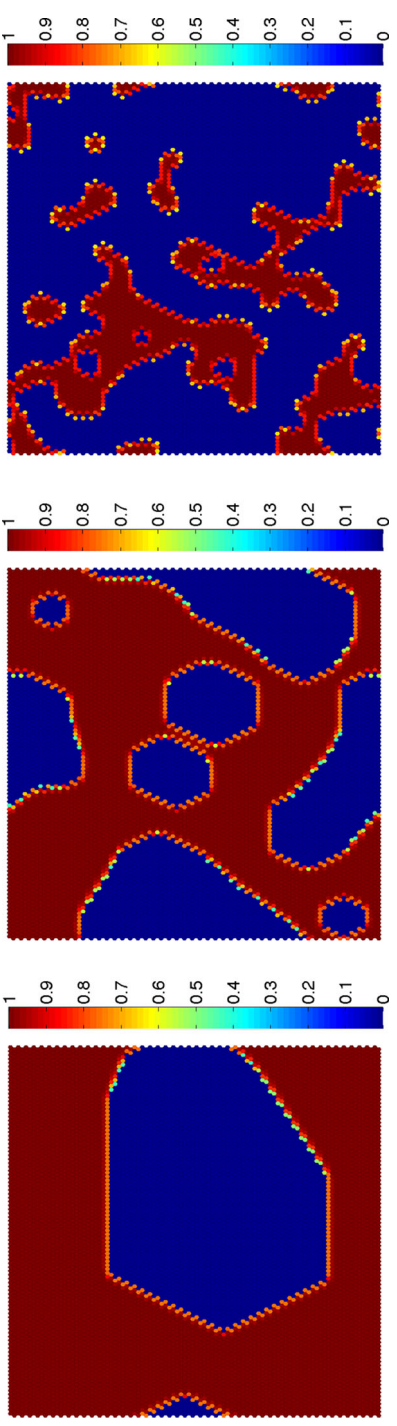

Fig. 10 Global coupling, hexagonal lattice, $\beta > 0$ instability. Cluster size dependence on number of positive eigenvalues, at steady state. *Left* to *right* $\kappa = 23.3$, $\kappa = 26$, $\kappa = 50$

3D checkerboard; in the $\beta > 0$, global coupling case, the largest eigenvalue is multiplicity six with eigenspace corresponding to the 3D long-wave modes. Subsequent eigenvalues crossing add higher frequency modes, again setting the VD length scale. Thus the cubic lattice is essentially identical to the square lattice case.

5 Numerical methods and parameters

Differential equations were solved numerically by Euler's method. Generic simulations employed random perturbations (normally distributed with standard deviation 0.001 mm) to break numerical meta-stability; artificially stabilized homogeneous simulations (Sect. 3.7) used no perturbation and exploited the meta-stability. Numerical partial derivatives of homogeneous solutions were computed using finite differences, and eigenvalues and eigenvectors were found with MATLAB's `eig()`, or `eigs()` for large systems.

Parameter values used throughout are $\rho = 2\,\mathrm{s}^{-1}$, $R_i = 0.058$ mm, $P_1 = 0.16$ cm H_2O, $P_2 = -27.6$ cm H_2O, $n_1 = 1$, $n_2 = 7$, $r_{imax} = 0.296$ mm, $P_{ref} = 10$ cm H_2O, $R_{ref} = R(P_{ref}) = 0.2792$ mm, $P_b = 10$ cm H_2O, and $A = 500(\mathrm{mm})^{-4}$, except where otherwise noted. It is worth noting that these parameters are illustrative and qualitatively similar behaviour exists across very large parts of parameter space, often extending orders of magnitude away. The Lambert model parameters for the airway wall are taken from Politi et al. (2010) for an order 1 airway. The airway luminal radius r is in mm. The ASM pressure κ has units cmH_2O. The flows Q, $\hat{Q}$ and q are obtained from Poiseuille flow considered independent of dynamic viscosity and tube length, formally with units $(\mathrm{mm}^3)/s$ where $\pi/(8\mu_{dv}L) = 1(\mathrm{cm\ H_2O\ s\ mm})^{-1}$ and $P_0 = 0$.

6 Discussion

We have presented a new lattice model consisting of identical elements representing terminal airway units. The lattice elements have nearest-neighbour coupling in all cases, and an optional all-to-all global coupling depending on the type of breathing control considered. The model neglects the branching airway structure and other mechanisms which might organise the spatial structure and instead focuses on the possible formation of clustered ventilation defects due to these types of coupling. We have studied the resulting lattice dynamical system for the purpose of finding both the conditions of clustered VDs, and the role that they may play.

The lattice DS arising from this model is an intrinsically discrete system due to the structure of the acini and connected terminal airways within the lung; it does not become a PDE in the limit of small lattice spacing. Such systems have of course been studied by others in many different contexts and lattice systems have a long history in mathematical biology (e.g. Keener 1987; Ermentrout and Edelstein-Keshet 1993). In general we are not able to make use of many of the convenient assumptions making certain types of analysis possible. For example, the local coupling is not of additive or diffusive type (Plahte 2001; Nekorkin et al. 1997), nor are we interested only in balanced heterogeneous patterns (Wang and Golubitsky 2005). Moreover the

complex form of the model nonlinearity does not even admit explicit solutions for the fixed points. However, the structure of the spectra and corresponding eigenspaces allows us to deduce much about the behaviour of the system from the sign of the relevant partial derivatives at the homogeneous equilibrium.

This allows us to consider the emergence of clustered ventilation defects, and the role played by different assumptions about breathing control. In particular we show that clustered VDs do emerge in the case including global coupling (the case where driving pressure increases to counteract constriction and maintain flow), and that the characteristic length scale of the emergent clusters is determined by the number of unstable eigenvalues, by way of each additional eigenvalue bringing higher frequency unstable modes. In the local coupling only case, the homogeneous solution appears to be stable for the physiological range of parameters space, however not universally so. There is at least one (aphysical) part of parameter space where the homogeneous solution gives way to a checkerboard solution, but there are no known clustered solutions.

We extended the model and analysis to consider the hexagonal and cubic lattice extensions, showing that both the hexagonal and cubic lattice models generate clustered VDs in the global coupling, $\beta > 0$ case in qualitatively the same way as the square lattice. In the local coupling only case, neither extension generated clustered VDs; in fact, the stability boundaries remain the same so that the parameter search for the square lattice model is valid for all three. That is, no parameters were found for which local-only coupling produces clustered ventilation defects. In the aphysical, $\beta < 0$, local-only case, there is a difference in the hexagonal lattice. Here the stability boundary is slightly different, and the shortwave instability is qualitatively different from the checkerboard solution. On the other hand, the cubic lattice model produces a 3D checkerboard in much the same way as the square lattice case.

When comparing clustered solutions seen in the model and those obtained experimentally, e.g. Tzeng et al. (2009), there are several factors to keep in mind. First is that the model is idealized and designed to consider the action of this particular method of spatial coupling; this is not to suggest that there are no other factors at work. For example, in real lungs there certainly are structural factors at work, even if dynamic phenomena are dominant, while we have considered only dynamic phenomena. For instance, we have made no attempt to capture either gravitational dependence or lobar structure, while both certainly play some role in determining experimental ventilation distributions. Similarly, it is not clear at what point in time one should compare, as we have defined the timescale arbitrarily—are experimental images taken near steady state, or are they a snapshot of dynamic equilibration? In the former case, the model suggests bimodal distributions with very narrow modes and very little in between, in contrast to most imaging data. However, if the system is still in the midst of equilibration, we might expect to see much broader distributions (e.g. Fig. 3). Given that breathing is inherently a dynamic process, the latter is a reasonable interpretation, though we have made no effort to explicitly model this much more complex situation.

Several other key modelling assumptions deserve extra discussion. One is neglecting the airway tree structure and considering only terminal units with identical input conditions. This assumption potentially neglects important contributions from the airway tree structure to overall VD formation. However, a first step is to understand how

clustered VDs might form from effects on the terminal units only, and this formulation allows a great deal more analysis and understanding. Incorporating the airway tree structure, and understanding its contribution, is an important area for future work. We emphasize that other explanations for clustered ventilation defects have been offered (e.g. Tgavalekos et al. 2005; Venegas et al. 2005); we have considered only one possible explanation in this model, and conclusions from its analysis are only valid in that context.

We note that the proposed coupling mechanism is not that in the recent work of Ma et al. (2013a,b) and Ma and Bates (2014) where direct mechanical strain is considered and airway–airway interactions via the parenchyma are shown to be limited. Here we are considering how parenchymal inflation is altered by constriction of supplying airways. Still, the coupling coefficient A which describes the strength of this interaction is not known. However, to a certain extent many of the results presented here can be viewed in a more general context than the specific model presented here. That is, the analysis of the eigenstructure relies only on the partial derivatives α, β and γ representing internal dynamics, nearest neighbour coupling, and global (all-to-all) coupling, respectively. These results are independent of the specific choice of model, but depend only on the coupling structure. Of course the model specifics play a role both in the conditions under which these instabilities occur, and also the stability of the resulting heterogeneous pattern.

One physiological question which naturally arises is the efficiency of clustered VD solutions. That is, would stabilizing the homogeneous solution be beneficial to an asthmatic patient? Model results suggest that while large clusters are inefficient, requiring greater driving pressure for equal total flow, smaller clusters are an efficient response to airway constriction, requiring less driving pressure than the stabilized homogeneous solution.

There are a number of areas where model assumptions leave room for important future work. One question is the possibility of simplification which retains the qualitative behaviour while allowing explicit fixed point solutions. This raises the prospect of showing conclusively that local-only instabilities are not of clustered VD type.

One might also wish to understand the role of the branching airway structure which was neglected in the model construction, or a more realistic breathing control model than two naïve approaches assumed here. Both remain important areas for future work. Nonetheless the lattice-based model and analysis presented here demonstrate the potential of this approach to answer important questions about the formation of clustered ventilation defects.

Acknowledgments The authors acknowledge the helpful comments of Claire Postlethwaite with regard to the structure of the eigenvalues and eigenvectors of the Jacobian.

References

Affonce DA, Lutchen KR (2006) New perspectives on the mechanical basis for airway hyperreactivity and airway hypersensitivity in asthma. J Appl Physiol 101:1710–1719

Anafi RC, Wilson TA (2001) Airway stability and heterogeneity in the constricted lung. J Appl Physiol 91(3):1185–1192

Bilek AM, Dee KC, Gaver DP (2003) Mechanisms of surface-tension-induced epithelial cell damage in a model of pulmonary airway reopening. J Appl Physiol 94(2):770–783
Donovan GM, Sneyd J, Tawhai MH (2012) The importance of synergy between deep inspirations and fluidization in reversing airway closure. PloS one 7(11)
Ermentrout BG, Edelstein-Keshet L (1993) Cellular automata approaches to biological modeling. J Theor Biol 160(1):97–133
Horsfield K, Dart G, Olson DE, Filley GF, Cumming G (1971) Models of the human bronchial tree. J Appl Physiol 31:207–217
Kay SS, Bilek AM, Dee KC, Gaver DP (2004) Pressure gradient, not exposure duration, determines the extent of epithelial cell damage in a model of pulmonary airway reopening. J Appl Physiol 97(1):269–276
Keener JP (1987) propagation and its failure in coupled systems of discrete excitable cells. SIAM J Appl Math 47(3):556–572
Lai-Fook SJ (1979) A continuum mechanics analysis of pulmonary vascular interdependence in isolated dog lobes. J Appl Physiol 46:419–429
Lambert RK, Wilson TA, Hyatt RE, Rodarte JR (1982) A computational model for expiratory flow. J Appl Physiol 52:44–56
Ma B, Sanderson M, Bates JHT (2013) Airway-parenchymal interdependence in the lung slice. Resp Physiol Meurobiol 185(2):211–216
Ma B, Breen B, Bates JHT (2013) Influence of parenchymal heterogeneity on airway-parenchymal interdependence. Resp Physiol Neurobiol 188(2):94–101
Ma B, Bates JHT (2014) Mechanical interactions between adjacent airways in the lung. J Appl Physiol 116:628–634
Nekorkin VI, Makarov VA, Kazantsev VB, Velarde MG (1997) Spatial disorder and pattern formation in lattices of coupled bistable elements. Phys D Nonlinear Phenom 100(3):330–342
Plahte E (2001) Pattern formation in discrete cell lattices. J Math Biol 43(5):411–445
Politi AZ, Donovan GM, Tawhai MH, Sanderson MJ, Lauzon AM, Bates JHT, Sneyd J (2010) A multiscale, spatially distributed model of asthmatic airway hyper-responsiveness. J Theor Biol 266(4):614–624
Rodriguez-Roisin R, Antoni F, Daniel N, Agusti AG, Wagner PD, Roca J (1991) Ventilation-perfusion mismatch after methacholine challenge in patients with mild bronchial asthma. Am Rev Resp Dis 144(1):88
Skander L, Porra L, Albu G, Trouillet N, Suhonen H, Peták F, Sevestre H, Suortti P, Sovijärvi A, Habre W et al (2013) Role of cellular effectors in the emergence of ventilation defects during allergic bronchoconstriction. J Appl Physiol 115(7):1057–1064
Tee GJ (1963) A novel finite-difference approximation to the biharmonic operator. Comput J 6(2):177–192
Tee GJ (2007) Eigenvectors of block circulant and alternating circulant matrices. N Z J Math 36:195–211
Tgavalekos NT, Tawhai M, Scott Harris R, Mush G, Vidal-Melo M, Venegas JG, Lutchen KR (2005) identifying airways responsible for heterogeneous ventilation and mechanical dysfunction in asthma: an image functional modeling approach. J Appl Physiol 99(6):2388–2397
Thorpe WC, Bates JHT (1997) Effect of stochastic heterogeneity on lung impedance during acute bronchoconstriction: a model analysis. J Appl Physiol 82(5):1616–1625
Tzeng Y-S, Lutchen K, Albert M (2009) The difference in ventilation heterogeneity between asthmatic and healthy subjects quantified using hyperpolarized 3he mri. J Appl Physiol 106(3):813–822
Venegas JG, Winkler T, Musch G, Vidal Melo MF, Layfield D, Tgavalekos N, Fischman AJ, Callahan RJ, Giacomo B, Scott HR (2005) Self-organized patchiness in asthma as a prelude to catastrophic shifts. Nature 434(7034):777–782
Wagner PD, Hedenstierna G, Bylin G (1987) Ventilation-perfusion inequality in chronic asthma. Am Rev Resp Dis 136(3):605–612
Wang Y, Golubitsky M (2005) Two-colour patterns of synchrony in lattice dynamical systems. Nonlinearity 18(2):631
World Health Organization (2007) Global surveillance, prevention and control of chronic respiratory diseases: a comprehensive approach
Yalcin HC, Perry SF, Ghadiali SN (2007) Influence of airway diameter and cell confluence on epithelial cell injury in an in vitro model of airway reopening. J Appl Physiol 103(5):1796–1807